
Heave Compensated Tripping

Morten Lie

December 16, 2018

NTNU - Norwegian University of Science and Technology
Faculty of Information Technology and Electrical Engineering
Department of Technical Cybernetics
TTK4550 - Specialization Project



PROSJEKTOPPGAVE

Kandidatens navn: Morten Lie
Fag: Teknisk Kybernetikk
Oppgavens tittel: Heave compensated tripping

Bakgrunn

When drilling, the hoisting is heave compensated to ensure steady drilling with a constant weight on bit even when the floating rig is moving up and down with the waves. When tripping, that is pulling the drillstring out of the hole/lowering into the hole, no such compensation is used, with the result of surge/swab effects downhole causing pressure variations and potential influxes or losses. The objective of this project work is to design a control system that isolates the string movement from rig heave, so that tripping can be performed smoothly without significant downhole pressure oscillations. The followings tasks should be addressed by the student:

1. Review the hoisting system and describe how it works today. Consider inputs and outputs for a potential control system for tripping.
2. Familiarize yourself with a model with flexible drill string, non Newtonian mud, rig motion, etc (MATLAB code to be provided), and set it up for simulation of tripping of one section (ca 30m). Make and document any necessary modifications to the code for this scenario.
3. Develop a controller to compensate heave motion with active hoisting: consider feedback e.g. on hook load or feedforward using measurements from motion sensor.
4. Add functionality to maximize tripping speed given min/max downhole pressures (drilling window).
5. Write report.

Faglærer/Veileder: Professor Ole Morten Aamo

Summary

Drilling oil wells from floating rigs introduces challenges that constantly pushes technology forward, and requires new ways of thinking. The objective of this work is to introduce a heave compensation control design that minimizes the pressure fluctuation in the well under hoisting operations. The pressure fluctuation is minimized by feeding measurements of the rigs heave motion into an algorithm that controls the hoisting system. To simulate the control design, a mathematical model is derived for the main components that are used under such operations. This work focuses on testing and validating a set of control designs that utilizes the hoisting system on the rig for heave compensation. Results suggests that the least sophisticated control design outperform the more sophisticated ones. Comprehensive simulations with different sea states and a variety of system parameters are discussed in this work, as well as a detailed comparison of the proposed control designs.

Table of Contents

Summary	i
Table of Contents	iii
List of Figures	v
Nomenclature	vii
1 Introduction	1
1.1 Background and motivation	1
1.2 Outline	1
2 Modelling	2
2.1 Introduction	2
2.2 Hoisting system	2
2.3 Drill string	6
2.4 Well	8
3 Simulator setup	11
3.1 Introduction	11
3.2 Boundary conditions	11
3.3 Wave model	15
3.4 Simulator parameters	16
4 Control system design and analysis	17
4.1 Introduction	17
4.2 System inputs	17
4.3 Control system designs	18
4.3.1 Alpha design	19
4.3.2 Bravo design	22
4.3.3 Charlie design	25

4.3.4	Control design comparison	28
5	Conclusion	30
	Bibliography	30

List of Figures

2.1	Drawworks hosting system schematic.	3
2.2	Block and tackle principle illustrated with a few variations of load cell locations, adopted from [2].	4
2.3	Electrical motor circuit , adopted from [8].	5
2.4	Characteristics of the drawworks "ADS-10SD with two 1150 HP AC motors" manufactured by National Oilwell Varco, adopted from [15].	7
2.5	Traveling block, adopted from [1].	8
2.6	Bottom hole assembly, adopted from [1].	9
2.7	Well schematic, adopted from [12].	10
3.1	Mud pump flow rate trajectory, $q_{mp}(t)$	12
3.2	Reference trajectory for tripping velocity, $v_{dr}(t)$	13
3.3	Thorsethaugen spectrum with a variety of peak frequencies, $H_s = 6m$	15
3.4	Thorsethaugen spectrum and RAO with $H_s = 6m$ and $\omega_0 = \frac{2\pi}{12}$	16
4.1	Motion reference unit from Kongsberg used to measure the rigs heave velocity, v_{rig} . [9]	18
4.2	Control design Alpha block diagram.	19
4.3	Alpha simulation without wave interaction measured $\bar{e}_d = 1.05 \cdot 10^{-3}$ m/s and $\Delta p_{bb} = 1.68$ Bar.	20
4.4	Alpha simulation with wave interaction measured $\bar{e}_d = 0.0293$ m/s and $\Delta p_{bb} = 3.93$ Bar.	21
4.5	Control design Bravo block diagram.	23
4.6	Bravo simulation without wave interaction measured $\bar{e}_d = 0.00798$ m/s and $\Delta p_{bb} = 1.62$ Bar.	24
4.7	Bravo simulation with wave interaction measured $\bar{e}_d = 0.0375$ m/s and $\Delta p_{bb} = 4.01$ Bar.	24
4.8	Control design Charlie block diagram.	26

4.9	Charlie simulation without wave interaction measured $\bar{e}_d = 0.00797$ m/s and $\Delta p_{bb} = 1.62$ Bar.	26
4.10	Alpha simulation with wave interaction measured $\bar{e}_d = 0.0351$ m/s and $\Delta p_{bb} = 4.01$ Bar.	27
4.11	Control design comparison with multiple parameter variations.	28

Nomenclature

Greek letters

μ	Kinematic friction coefficient
ω	Angular velocity, rad/s
ϕ	Azimuth, rad
ρ	Density, kg/m ³
σ	Stress, Pa
θ	Inclination, rad

Latin letters

A	Cross section area, m ²
E	Elasticity constant
g	Gravitational acceleration, m/s ²
L	Length, m
m	Mass, kg
p	Pressure, Pa
q	Flow rate, m ³ /s
r	Radius, m
t	Time, s
v	Velocity, m/s
x	Axial position, m

Subscripts

<i>a</i>	Mud in annulus
<i>atm</i>	Atmospheric pressure, 10^5 Pa
<i>bb</i>	Below bit
<i>BHA</i>	Bottom Hole Assembly
<i>d</i>	Drill string
<i>dw</i>	Drawworks
<i>hl</i>	Hook load
<i>i</i>	Mud inside the drill string
<i>lp</i>	Low pass
<i>mp</i>	Mud pump
<i>r</i>	Reference
<i>TFA</i>	Total Flow Area
<i>w</i>	Well

Introduction

1.1 Background and motivation

When drilling into a petroleum reservoir from a floating rig, it is critical that the down hole pressure is maintained within a required pressure margin in order to avoid damages to the well. Pressure fluctuations beyond the pore - and fracture pressure may harm the structural integrity of the well, and may lead to costly damages. A great amount of research has been done on this subject matter, and a lot of control strategies has been developed to manage the pressure down hole utilizing a set of fluid control devices on the topside of the well and on deck. In this work, a heave compensation control strategy utilizing the hoisting system on deck is introduced. The objective is to minimize the pressure fluctuation down hole caused by the heave motion of the rig, induced by the waves. The controller will be designed to reduce the heave motion of the drill string when moving it up and down inside the well. This is known as tripping. A successful heave compensation control system will make it possible to drill wells with tight pressure windows in rough weather conditions in the future.

1.2 Outline

This report is divided into several chapters. First, an introduction of the main components involved during the drilling operations is presented in Chapter 2, including a mathematical model for the respective component. Then, Chapter 3 moves on to discuss the setup of the simulator that was used to test and validate the heave compensation control designs. Further, in Chapter 4, the control system designs are presented, simulated and validated. Lastly, in Chapter 5, a conclusion of this work takes place.

Modelling

2.1 Introduction

This chapter will focus on the main components that are necessary to model for simulation and validation of the heave compensation control design in Chapter 4. First, the hoisting system on the rig will be discussed, followed by a brief discussion about the model for the drill string and the well.

The models in this work are described using both body and inertial reference frames. The hoisting system, which is mounted to the rig, is modelled using the rig body frame. The transition between the inertial frame and the rig body frame is assumed to be a simple translational transformation. The hoisting system is assumed to be located at close proximity of the rigs center of gravity, so that the attitude of the rig will not be taken into account. Further, the drill string dynamics as well as the fluid dynamics in the well are described using an inertial reference frame.

2.2 Hoisting system

In order to perform tripping, that is raising and lowering the drill string, a hoisting system capable of handling heavy loads is necessary. The hoisting system should have a workspace over 30 meters, since this is the length of each pipe segment that makes up the total length of the drill string. The hoisting system will be used as the actuator organ for the heave compensation control algorithm, which will be discussed in Chapter 4. According to [3], there are multiple types of hoisting systems operating on modern rigs today. One of the more common hoisting system for rotary drilling rigs is the drawworks hosting system, which will be reviewed in the following section.

The drawworks hoisting system is based on the block and tackle principle which consists of a drawworks module, a crown block, a traveling block, a drill line and multiple sheaves as well as load cells used to estimate hook load (see Figure 2.1 and 2.2). The drawworks consists of a motor, either electric or hydraulic, which is connected to a drum

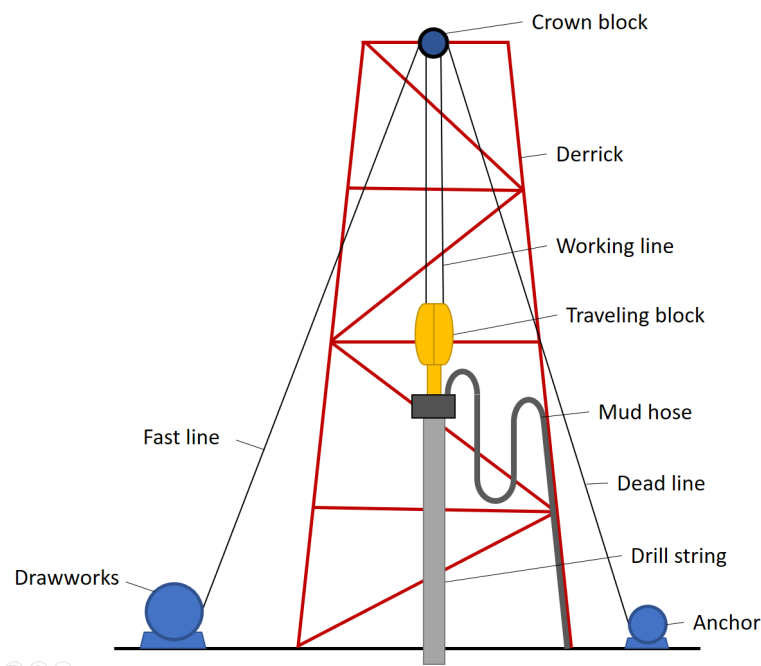


Figure 2.1: Drawworks hosting system schematic.

for the drill line through a transmission system and breaks. The drill line is commonly divided into three parts; fast line, working lines and dead line. The fast line is the part of the drill line that connects the drawworks to the last sheave in the tackle system. The fast line will move at a speed of $v = \omega r$ where ω is the angular velocity of the drum and r is the radius to the outer drill line layer in the drum. Further, the working lines are connected through an even number of sheaves between the crown block and the traveling block. Lastly, the dead line is the length of the drill line from the first sheave in the crown block and down to the dead line anchor sitting on the drilling deck across from the drawworks drum. The first sheave in the crown is called the dead-line sheave, and will be stationary regardless of the state of the system. When the motor pulls drill line into the drum, the traveling block is raised up towards the crown block at a speed depending on the number of working lines in the arrangement. Since the power needed to raise a given load increases quadratically with velocity, it is necessary to have sufficiently powerful motors to avoid power losses which could result in undesired movements of the drill string. The mechanical tension in the fast line is reduced by the number of working line pairs in the configuration. However, the friction force in the sheaves will be more significant for an increase of working line pairs. Consequently, one would need a more sophisticated model to estimate the hook load for these configurations.

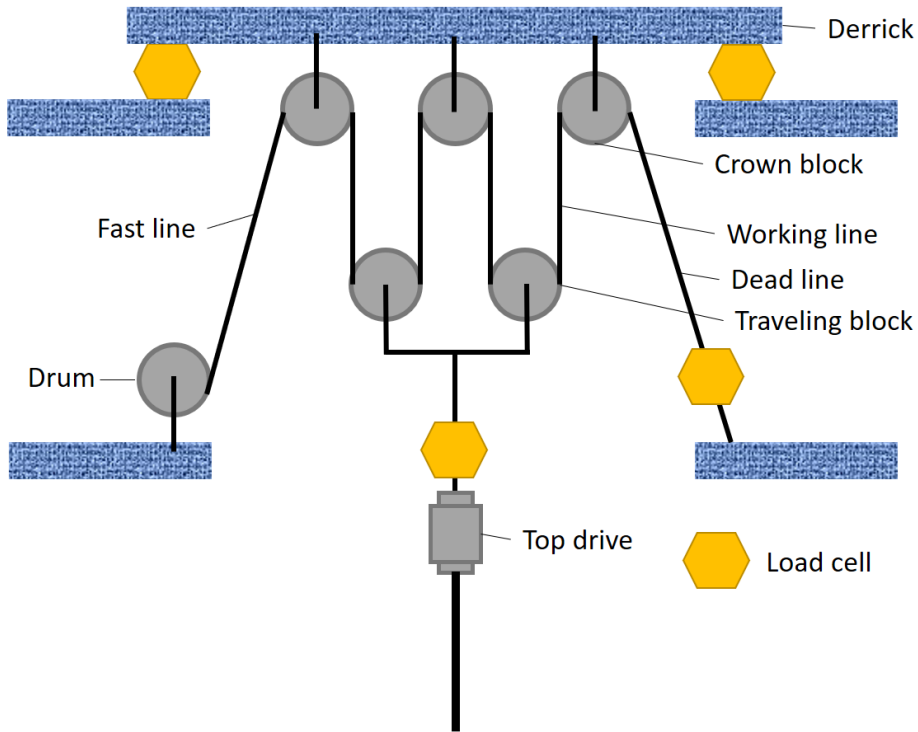


Figure 2.2: Block and tackle principle illustrated with a few variations of load cell locations, adopted from [2].

Hook load estimate

Typically, the load cells used to calculate the hook load are placed quite far away from the top of the drill string. The position of the load cells may influence the accuracy of the hook load estimates. The most common location of the load cells is at the dead line anchor, where the hook load can be calculated based on the number of working lines in the configuration. Other locations that are used for load cell placement are at the top of the derrick, in the crown block, and above the top drive. Factors like friction will influence the measurements of hook load, which may vary based on the tilt angle of the traveling block. Also the mud hose plays a role for the hook load estimates, as the weight of the mud hose on the system depends on the position of the traveling block. The load from the mud hose can be estimated by assuming the mud hose is suspended between two points and follows a catenary curve which has the form

$$y = a \cosh\left(\frac{x}{a}\right) \quad (2.1)$$

where the mud hose crosses the y-axis at its lowest point. a is a curve parameter and $\cosh(\cdot)$ is the hyperbolic cosine function.

Hoisting system model

As previously described, the hoisting system consists of a motor attached to the line through a wire drum that runs the hoisting system. In this work, we assume that the drawworks can be modelled as a first order system with one time constant describing the response. Since our main interest is the phase shift caused by the response of the hoisting system, approximating the system to a first order can be argued as satisfactory. Later in this paper, the control design will be discussed where the response time of the hoisting system is an important factor for how well the control system compensates for the heave motion. The following assumptions have been made when modelling the hoisting system.

- Friction forces in the sheaves and gears are neglected
- Elasticity in the wires is neglected
- Tilt angle of the blocks is assumed to have no effect
- Tension exerted by the mud hose and top-drive umbilical are neglected

With these assumptions, the hoisting system model encapsulates the dynamics of the electric motor and the velocity change caused by the crown and tackle system. The dynamics of an electric motor can be modelled using a simple RL circuit, displayed in Figure 2.3. The mechanical torque caused by electrifying the windings in the motor is assumed

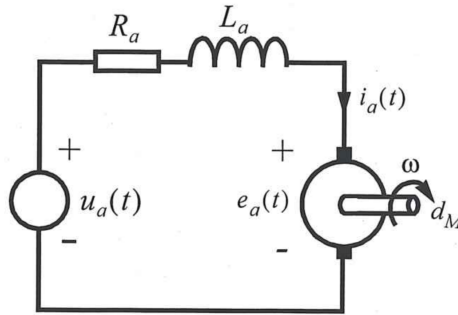


Figure 2.3: Electrical motor circuit , adopted from [8].

to be proportional to the current flowing in the circuit. Mathematically we express this relationship as

$$M_{el} = K_T i_a \quad (2.2)$$

where K_T is a proportionality constant. When the motor is rotating, a voltage is induced in the windings which is proportional to the angular velocity of the rotor. Again we express this relationship as

$$e_a = K_v \omega \quad (2.3)$$

where K_v is a proportionality constant. Utilizing Kirchhoff's voltage law, the dynamics in the circuit of the motor can be expressed as

$$u_a = R_a i_a + L_a \frac{di_a}{dt} + e_a \quad (2.4)$$

Furthermore, the dynamics of the mechanical system can be expressed utilizing Newtons 2nd law for rotation

$$M_{el} - M_{load} - B\omega = J\dot{\omega} \quad (2.5)$$

where M_{load} is a torque caused by the load in the system and B and a linear damping caused by friction.

When simulating the hoisting system, we are interested in the dynamics from the applied voltage u_a to the angular velocity ω . Laplace transformation of Equation (2.4) and (2.5) yields the transfer function

$$H_{motor} = \frac{\omega}{u_a} = \frac{1}{K_v \left(1 + \frac{JR_a}{K_v K_T} s + \frac{JL_a}{K_v K_T} s^2 \right)} \quad (2.6)$$

Since the electric motor in the drawworks system is large (typically 1.5 - 3 mega watts), we assume that the mechanical time constant is sufficiently greater than the electrical time constant in the system. Thus, the electric motor can be simplified to a first order transfer function

$$H_{dw}(s) = \frac{v_{dw}}{u}(s) = \frac{K_{dw}}{T_{dw}s + 1} \quad (2.7)$$

where K_{dw} is a scaling constant capturing the velocity change from the rotating motor shaft to the velocity of the travelling block. The time constant is expressed as

$$T_{dw} = \frac{JR_a}{K_v K_t} \quad (2.8)$$

In this work, we base the hook load capacity and tripping velocity capability of the drawworks on those manufactured by National Oilwell Varco, which were recommended by Equinor. Specifically, the NOV ADS-10SD with two 1150 HP AC motors. The hook load to tripping velocity curve for this drawworks with 8, 10 and 12 working lines is displayed in Figure 2.4

2.3 Drill string

The hoisting system described in the previous section is used to manage the movement of the drill string. The traveling block, displayed in Figure 2.5, is holding the weight of the drill string. The drill string is used to transport drilling mud into the well during drilling operations which cools the drill bit and transports rocks and other drilling debris to the surface. Furthermore, the drilling mud can also be used to control the pressure down hole. This will be discussed further in Chapter 3. The drill string consists of the bottom hole assembly (BHA), the transition pipe, and the drill pipe. As indicated in Figure 2.6, the BHA is made up by a drill bit used to break up rock formation below the sea bed, drill collars which are used to apply weight to the drill bit and drilling stabilizers which keep the assembly centered in the hole. The transition pipe is used for the transition between the BHA and the drill pipe. The drill pipe consists of multiple 30 meter segments that make up the pipe which goes from the bottom of the well and up to the rig.

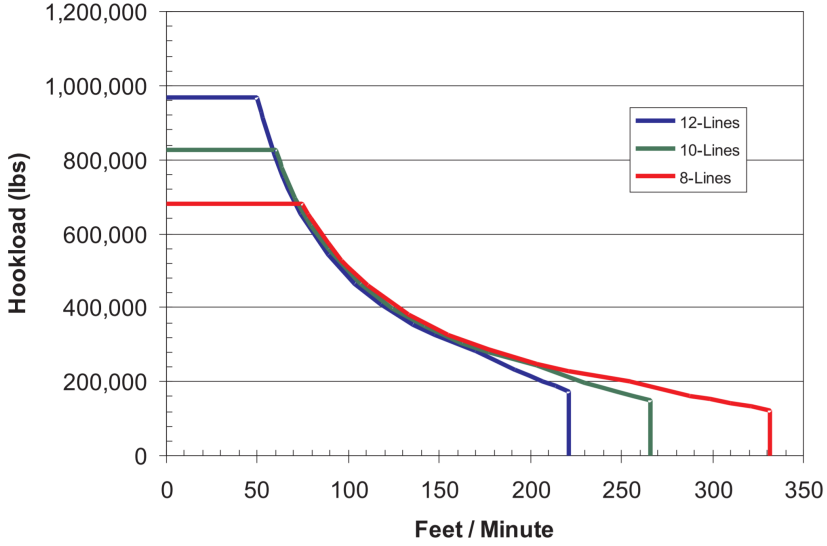


Figure 2.4: Characteristics of the drawworks "ADS-10SD with two 1150 HP AC motors" manufactured by National Oilwell Varco, adopted from [15].

Drill string model

Inspired by the work of [7], the drill string is modelled as a one dimensional elastic rod based on the 1D continuity equation.

$$\frac{\partial \sigma_d}{\partial t} = E \frac{\partial v_d}{\partial x} \quad (2.9)$$

$$\frac{\partial v_d}{\partial t} = \frac{1}{\rho_d} \left(\frac{\partial \sigma_d}{\partial x} - \frac{1}{A_d} (F_d(v_d, q_a, q_i) + F_{drag}) \right) - g \cos(\theta) \quad (2.10)$$

Following the work of Strecker and Aamo [13], the forces acting on the drill string, F_d and F_{drag} are modelled as follows. The first term comes from the mud inside the drill string and inside the annulus acting on the drill string, decomposed as

$$F_d(v_d, q_a, q_i) = -F_a(q_a, v_d) - F_i(q_i, v_d) \quad (2.11)$$

Further, the drag force F_{drag} can be modelled as

$$F_{drag} = \mu F_N \quad (2.12)$$

where μ is the kinematic friction coefficient and F_N is the normal force modeled as in [10]

$$F_N = \sqrt{\underbrace{\left(A_d \sigma_d \frac{\partial \phi}{\partial x} \sin \theta \right)^2}_{\text{Horizontal force}} + \underbrace{\left(m_d \sin \theta + A_d \sigma_d \frac{\partial \theta}{\partial x} \right)^2}_{\text{Vertical force}}} \quad (2.13)$$



Figure 2.5: Traveling block, adopted from [1].

The flow that runs through the drill bit at the end of the drill string can be modelled with a non-return valve equation where turbulent flow is assumed. The flow as a function of the pressure difference over the valve, Δp , is stated as in [4]

$$q_{bit}(\Delta p) = \begin{cases} C_d A_{TFA} \sqrt{\frac{2}{\rho_d} \Delta p}, & \text{if } p_i^{bit} > p_{bb}^{bit} \\ 0, & \text{if } p_i^{bit} \leq p_{bb}^{bit} \end{cases} \quad (2.14)$$

where C_d is the valve flow coefficient and A_{TFA} is the total flow area through the bit nozzles. The flow out of the drill bit goes into the annulus of the well which will be discussed next.

2.4 Well

The well is composed by the drill string with the drill bit at the end, a sealed annulus surrounding the drill string with a choke valve and a back pressure pump at the top. The well schematic is displayed in Figure 2.7. The drill string is lowered from a floating rig into the well, and mud is pumped through the drill string at a rate denoted as q_{mp} . The mud that is being pumped through the drill string serves as both cooling for the drill bit under drilling operations, as well as bottom hole pressure control. Further, the mud flows through the bit valve at the bottom of the drill string, and flows up the annulus and through the choke valve. The choke valve and the back pressure pump are controlled in order to minimize pressure fluctuations in the well. Furthermore, the velocity of the drill string is denoted v_{rig} , and is a resulting velocity of the waves acting on the rig, as well as the



Figure 2.6: Bottom hole assembly, adopted from [1].

controlled velocity from the hoisting system. As done in [10], the 1D continuity equation is used to model the well and the drill string system, which is expressed in equations (2.15) - (2.18). The flow inside the drill string and annulus is assumed to flow in the axial direction, which as illustrated in Figure 2.7, is in the up/down direction. The term $\frac{\beta}{A} \frac{\partial q}{\partial x}$ represents advective transport in the mass balance equations (2.15) and (2.17). The latter term in the mass balance, $\left(\frac{\beta}{A} \frac{\partial A}{\partial p}\right) \frac{\partial p}{\partial t}$, encapsulates the effect of compression of the annulus due to the pressure differential from the drill string. Further, Equation (2.16) and (2.18) represents the momentum balances. The forces present in the equations are due to the pressure gradient, friction and gravity, respectively.

$$\frac{\partial p_a}{\partial t} = -\frac{\beta_a}{A_a} \frac{\partial q_a}{\partial x} - \left(\frac{\beta_a}{A_a} \frac{\partial A_a}{\partial p_i}\right) \frac{\partial p_i}{\partial t} \quad (2.15)$$

$$\frac{\partial q_a}{\partial t} = -\frac{A_a}{\rho_a} \frac{\partial p_a}{\partial x} - \frac{1}{\rho_a} [F_{a,in}(q_a, v_i) + F_{a,out}(q_a, v_i)] - A_a g \cos(\theta) \quad (2.16)$$

$$\frac{\partial p_i}{\partial t} = -\frac{\beta_i}{A_i} \frac{\partial q_i}{\partial x} - \left(\frac{\beta_i}{A_i} \frac{\partial A_i}{\partial p_a}\right) \frac{\partial p_a}{\partial t} \quad (2.17)$$

$$\frac{\partial q_i}{\partial t} = -\frac{A_i}{\rho_i} \frac{\partial p_i}{\partial x} - \frac{1}{\rho_i} F_i(q_i, v_i) - A_i g \cos(\theta) \quad (2.18)$$

The model subscripts for fluid in the annulus and drill string are denoted a and i , respectively. The implementation of the model is done by distributing the hyperbolic partial differential equations over a uniform grid spanning the well and the drill string. The following assumptions were done when modelling the well.

- Constant parameters are assumed along each section of the distributed model
- Constant density is assumed inside the drill string and the annulus

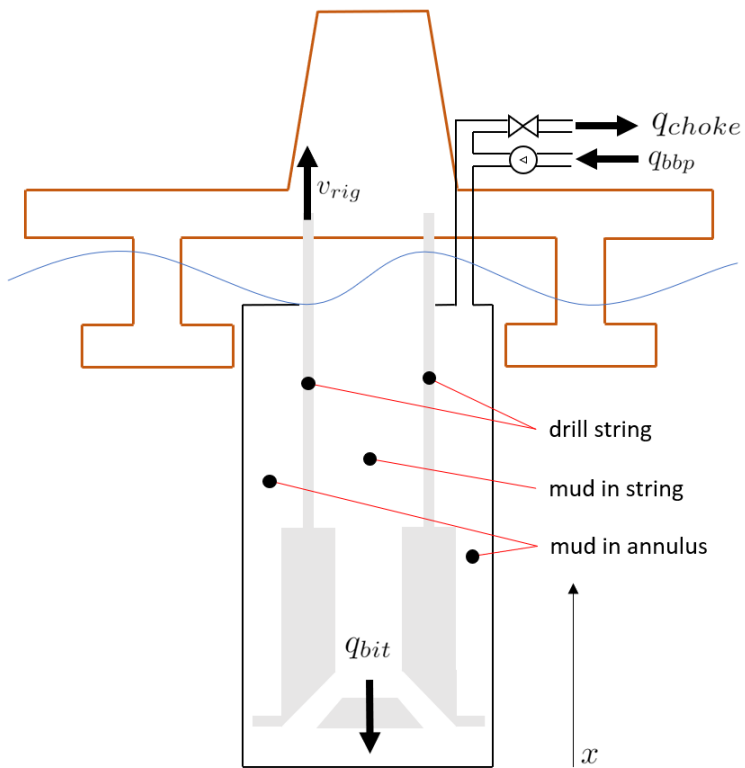


Figure 2.7: Well schematic, adopted from [12].

- BHA is a rigid body
- Thermal effects on dynamics are negligible
- There is no mud loss to the formation in the well

Simulator setup

3.1 Introduction

This chapter will describe the setup for the simulator used to simulate and validate the heave compensation control system. The simulator and the simulation setting in this work are based on the work of Strecher et al. (2017) [13]. The system of partial differential equations (2.15) - (2.18) was distributed over a finite grid for simulations of the drill string and the well. The number of pressure nodes used in the distribution was set to $N = 50$ where 5 of which were pressure nodes below the drilling bit. The boundary conditions for the simulation were set by the control strategy of the choke valve, the back pressure pump, the mud pump topside, and the velocity of the drill string. These boundary conditions will be further discussed throughout this chapter, where the drill string velocity is the main control organ for the heave compensation system. The simulation will focus on one drill string segment, i.e. the tripping distance will be 30 meters.

3.2 Boundary conditions

Mud pump topside

The mud pump topside has multiple functions. It is used to get grainy mud to the surface during drilling, the cooling the drill bit, and to control pressure inside the annulus. The objective for using this pump while tripping is pressure management. When raising the drill string towards the surface, the displaced volume by the drill string should be replaced with mud in order to maintain the pressure in the well. The pump is a simple mud pump where the complexity of the flow rate trajectory is constrained to be a simple function of time. Thus, a ramp function was implemented for this mud pump, where the flow rate is

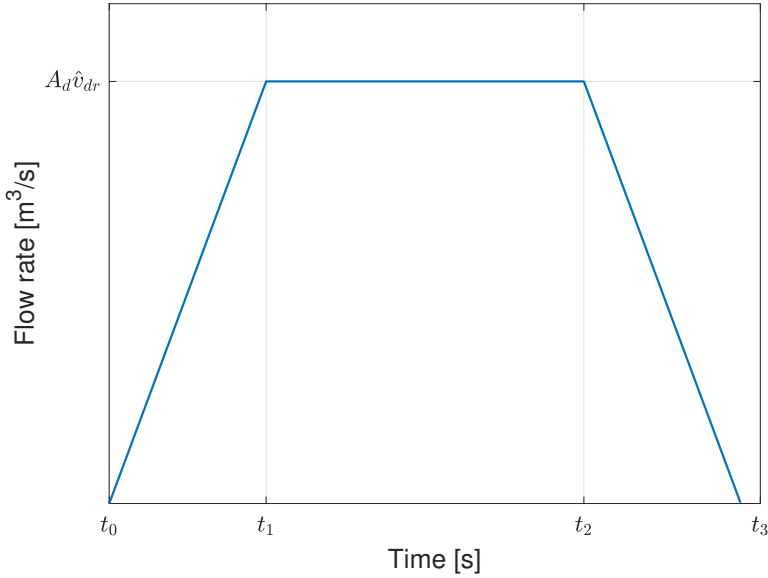


Figure 3.1: Mud pump flow rate trajectory, $q_{mp}(t)$.

expressed as

$$q_{mp}(t) = \begin{cases} \frac{A_d \hat{v}_{dr}}{t_1 - t_0} (t - t_0), & \text{if } t_1 > t > t_0 \\ A_d \hat{v}_{dr}, & \text{if } t_2 > t > t_1 \\ \frac{A_d \hat{v}_{dr}}{t_3 - t_2} (t_3 - t), & \text{if } t_3 > t > t_2 \end{cases} \quad (3.1)$$

where A_d is the outer area of the drill string, and \hat{v}_{dr} is the desired tripping velocity. The time intervals $t_i, i \in \{0, \dots, 3\}$ are decided based on the tripping velocity trajectory. A plot of this flow rate can be viewed in Figure 3.1.

Tripping velocity trajectory

In order to accomplish a smooth acceleration of the drill string, a calculation of an appropriate tripping velocity trajectory is necessary. Consider the following sigmoid function as a candidate for this reference trajectory

$$v_{dr}(t) = \begin{cases} \frac{\hat{v}_{dr}}{1 + e^{k(t_0 - t)}}, & \text{if } t_1 > t > t_0 \\ \hat{v}_{dr}, & \text{if } t_2 > t > t_1 \\ \frac{\hat{v}_{dr}}{1 + e^{-k(t_0 - t)}}, & \text{if } t_3 > t > t_2 \end{cases} \quad (3.2)$$

where \hat{v}_{dr} is the maximum tripping velocity. The reference trajectory is displayed in Figure 3.2. The reason for this candidate is the smoothness of the function, both in the beginning of the acceleration and when the velocity approaches \hat{v}_{dr} . It is also a simple function to implement in software, and it has a deterministic acceleration, adjusted by the constant k . As earlier discussed, one drill string segment has a length of $L_{dj} = 30$ meters. Thus,

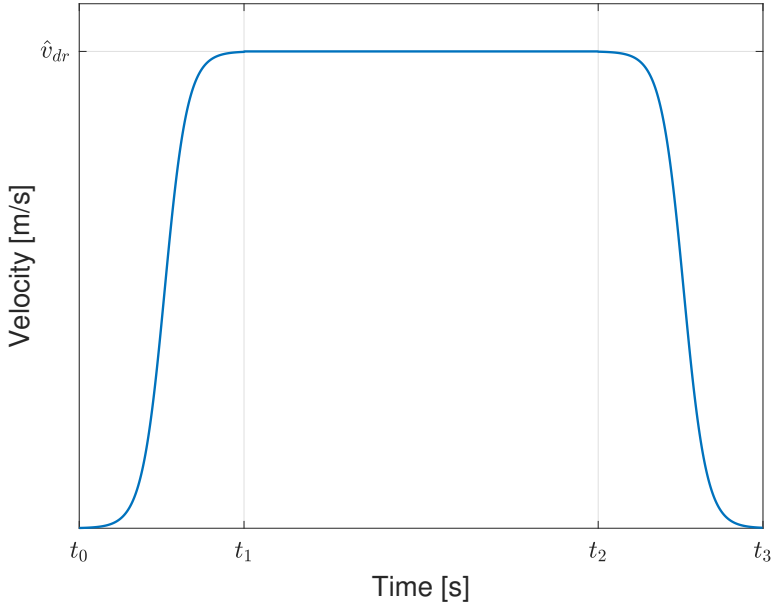


Figure 3.2: Reference trajectory for tripping velocity, $v_{dr}(t)$.

the algorithm generating this reference signal must make sure that the equality constraint

$$\int_{t_0}^{t_3} v_{dr}(t)dt = L_{dj} \quad (3.3)$$

is active.

Choke valve and back pressure pump control

Many managed pressure drilling (MPD) control strategies have been developed utilizing the choke valve and back pressure pump to maintain a certain pressure in the well. Bregholtz et al. (2010) [16] suggest using a model predictive control (MPC) approach to control the pressure down hole. Also Strecher et al. (2017) [12] suggest attenuation heave-induced pressure oscillations utilizing the choke valve and back pressure pump. According to Equinor, a more common setting for these actuators is to set them constant for a specific flow through the system. This method introduced quite dramatic pressure oscillations in the simulator. To minimize these oscillations caused by the tripping, as well as the pressure reflections from the annulus wall, the actuators were set for impedance matching as suggested in [13]. This is a relatively simple design to implement, and works quite effective for pressure oscillation reduction caused by other factors than the heave movement of the rig. The impedance matching regime is achieved by setting a reference annulus pressure p_{ar} at the top of the annulus, and by setting a reference flow rate q_{ar} . Based on the desired movement of the drill string and the mud pump top side, the reference flow rate can be set

to

$$q_{ar}(t) = A_d v_{dr}(t) - q_{mp}(t) \quad (3.4)$$

to minimize pressure fluctuations caused by tripping of the drill string. Further, to obtain impedance matching, the axial flow of the mud inside the annulus is expressed as

$$q_a = q_{ar}(t) + \frac{A_a}{\sqrt{\beta_a \rho_a}} (p_a^{top} - p_{ar}) \quad (3.5)$$

where p_a^{top} is the pressure inside the annulus at the top of the structure, i.e. where the valve is mounted. The flow through the choke valve is calculated by the valve equation

$$q_{choke} = C(u) \sqrt{\frac{2(p_a^{top} - p_{atm})}{\rho_a}} \quad (3.6)$$

where we are assuming atmospheric pressure at the outflow of the valve. Differentiating Equation (3.6) wrt. the reference pressure, we obtain

$$\left. \frac{\partial q_{choke}}{\partial p_a^{top}} \right|_{p_a^{top}=p_{ar}} = \frac{C(u)}{\sqrt{2\rho_a(p_{ar} - p_{atm})}} \quad (3.7)$$

According to [11], the optimal valve opening u^* is set such that

$$\frac{C(u^*)}{\sqrt{2\rho_a(p_{ar} - p_{atm})}} = \frac{A_a}{\sqrt{\beta_a \rho_a}} \quad (3.8)$$

With the following expression for the control equation of the valve, $C(u) = C_d u A_{valve}$ we get the optimal control strategy for the valve

$$u^* = \frac{1}{C_d} \sqrt{\frac{2(p_{ar} - p_{atm})}{\beta_a}} \quad (3.9)$$

in order to maintain impedance matching. By inserting this optimal valve opening into Equation 3.6, the choke flow becomes

$$q_{choke} = C(u^*) \sqrt{\frac{2(p_{ar} - p_{atm})}{\rho_a}} \quad (3.10)$$

The flow rate reference for the back pressure pump is set to

$$q_{bpp}(t) = q_{choke} - q_{ar}(t) \quad (3.11)$$

to obtain impedance matching by a passive boundary condition implemented by setting the flow rates through the choke valve and back pressure pump.

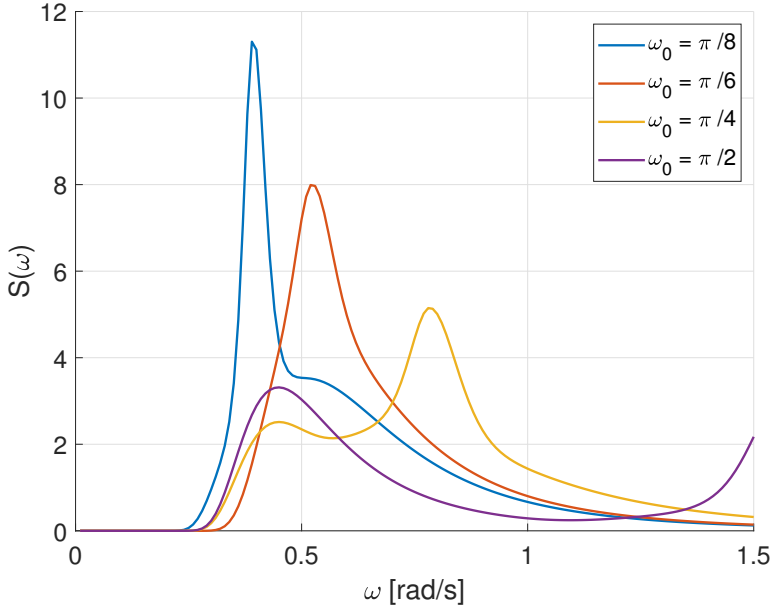


Figure 3.3: Thorsethaugen spectrum with a variety of peak frequencies, $H_s = 6m$.

3.3 Wave model

To simulate realistic heave motion, one would need a realistic model for the waves characterized by a spectrum of the wave elevation. The doubly peaked Thorsethaugen spectrum was developed specifically for the North Sea by curve fitting experimental data [14]. The spectrum includes both the effect of swell (low-frequency waves) and newly developed waves (high-frequency waves), and was standardized under the Norsok Standard (1999) [5]. The spectrum density function $S(\omega)$ is plotted in Figure 3.3 with a variety of peak frequencies and significant wave height of $H_s = 6m$. As one may observe in the figure, if the peak frequency ω_0 is chosen less than approximately 0.6 rad/s, the two peaks merge to one peak, becoming a spectrum where the swell dominates. The amplitude of the waves follow the relationship

$$A_k = \sqrt{2S(\omega_k)\Delta\omega} \quad (3.12)$$

where $\Delta\omega$ is a constant difference between the frequencies. Equation (3.12) is further used to compute wave-induced responses in the time domain for the simulation. However, the actual movement of the rig depends on the response amplitude specter (RAO). The rig response to the waves depends on the frequency, which is illustrated in Figure 3.4 where the rig response spectrum $R(\omega)$ is given by

$$R(\omega) = S(\omega)RAO(\omega)^2 \quad (3.13)$$

The RAO specter used in this work is based on values from the Aker H6e semi-submersible for ultra deep water and harsh environment. Most of the energy in the response spectrum is in the period range 10 - 15 seconds. Here the significant wave height H_s was set to 6

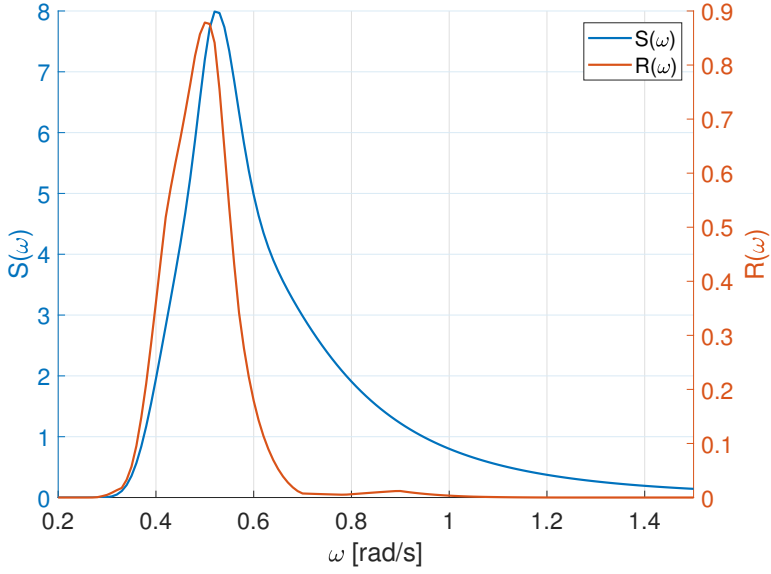


Figure 3.4: Thorsethaugen spectrum and RAO with $H_s = 6m$ and $\omega_0 = \frac{2\pi}{12}$.

meters and the peak frequency $\omega_0 = \frac{2\pi}{T_0}$, where the peak period T_0 was set to 12 seconds. In the simulator, the frequency range is divided up in an equidistant grid of N frequencies where the wave frequency vector $\omega = [\omega_1, \omega_2, \dots, \omega_N]$ was used in superposition to get the heave motion x_{rig} of the drilling rig.

$$x_{rig} = \sum_{k=1}^N \sqrt{2R(\omega_k)\Delta\omega} \sin(\omega_k t + \phi_k) \quad (3.14)$$

where ϕ_k is generated randomly from a uniform distribution on the interval $[0, 2\pi]$ in the simulator.

3.4 Simulator parameters

The configuration of the simulator was based on the values in Table 3.1.

L_d	4000 m	μ	0.2	ρ_d	1500 kg/m ³
L_{BHA}	100 m	θ	0 rad	ρ_a	1500 kg/m ³
E	206.8 GPa	g	9.81 m/s ²	ρ_{bb}	1500 kg/m ³
A_d	9.4×10^{-3} m	m_d	30 kg/segment	β_{bb}	1.8 GPa
A_w	3.66×10^{-2} m	m_{BHA}	12000 kg	β_d	1.8 GPa
A_{TFA}	9.4×10^{-3} m	ϕ	0 rad	β_a	1.6 GPa
C_d	0.98	dt	0.1 s		

Table 3.1: Parameter list

Control system design and analysis

4.1 Introduction

In this chapter, the system inputs for the control designs will be discussed, and three control designs will be defined, simulated and validated. The control designs were implemented in Matlab as an extension to the Matlab code provided for simulation of the drill string and well dynamics.

4.2 System inputs

Motion reference unit

The motion reference unit (MRU) will be used to inform the control system about the state of the rig. The MRU is usually placed close to the center of gravity of the rig to simplify computation. Kongsbergs fifth generation MRU will be considered in this work which gives high precision measurements of the 3 axis accelerations of the rig, heave velocity as well as angular orientations and angular rates. However, the measurements that will be necessary for this work is the heave velocity, v_{rig} . This will be used to cancel the heave induced movements of the rig in a feed forward loop, further discussed in Section 4.3. The measured heave velocity is contaminated with measurement noise which contributes with a root mean squared value of 0.01 m/s to the signal. The input can be modeled as

$$v_{MRU} = v_{rig} + \omega_{MRU} \tag{4.1}$$

where the noise ω_{MRU} is assumed to be Gaussian distributed noise with expected value $\mu = 0$ and standard deviation $\sigma = 0.01$ m/s, and the signal bias is assumed to be zero. According to Equinor, the signal from the MRU is updated at a rate of 10Hz.



Figure 4.1: Motion reference unit from Kongsberg used to measure the rigs heave velocity, v_{rig} . [9]

Hook load estimation

The hook load is a nontrivial measurement to obtain, as discussed in [3]. However, for simplification, we assume that the measurement is based on load cells mounted above the top drive, so that the friction forces from the sheaves can be neglected. In the simulator, the measurement is calculated based on the stress that the drill string is experiencing. The hook load is calculated as

$$F_{hl} = A_d p_d \quad (4.2)$$

where A_d is the drill string area, and p_d is the external pressure on the drill string.

4.3 Control system designs

In this work, three different control designs were implemented and tested. These designs will be presented in this section along with simulation and performance analysis. The names of the control systems are motivated by the first three letters in the phonetic alphabet. The control designs were implemented in Matlab script, but for illustrative purposes, the control designs are displayed as block diagrams implemented in Simulink.

The following simulations were done with each control system to validate their respective performances. First, the systems were simulated without interaction of waves, and then with wave interaction based on the Torsethaugen spectrum. Validation of the performance is mainly based on the change in pressure down hole, denoted Δp_{bb} . This value is calculated as the difference between the maximum pressure and minimum pressure below the drilling bit that was observed during the simulation. According to [6], a typical bench mark is a delta pressure that satisfies $|\Delta p_{bb}| < 2.5$ Bar. In addition, the root mean squared (RMS) of the tripping velocity error will be computed and compared between the respective control designs. The RMS of the tripping velocity error, denoted \bar{e}_d , is calculated as

$$\bar{e}_d = \sqrt{\frac{1}{t_3 - t_0} \int_{t_0}^{t_3} (v_{dr}(\tau) - v_d(\tau))^2 d\tau} \quad (4.3)$$

Each control design will now be presented, and simulated under the scenario described in Chapter 3. The drawworks time constant was set to $T_{dw} = 0.3$ s, the tripping velocity was chosen as $\hat{v}_{dr} = 0.2$ m/s based on the drawworks characteristics in Figure 2.4, and the significant wave height was set to $H_s = 6$ m. The update frequency of the control loop was set to 10 Hz.

4.3.1 Alpha design

The first control design to be discussed contains only one control loop, namely a speed controller for the drawworks system. The drawworks system is assumed to be implemented with an encoder which returns the angular velocity of the motor, denoted ω_{dw} . The speed of the motor is typically controlled with a variable speed drive (VSD) which regulates the frequency of the AC voltage that is supplied to the three phase asynchronous electric motor. Usually the VSDs are compatible with most encoders, such that the speed controller can be implemented in the VSD. The controller is assumed to be properly tuned, such that the dynamics of the drawworks system can be assumed to be approximated with the first order transfer function previously mentioned in Equation (2.7), restated here

$$H_{dw} = \frac{v_{dw}}{u} = \frac{K_{dw}}{T_{dw}s + 1} \quad (4.4)$$

The wave interaction is modelled as a disturbance input to the system, and is damped by the MRU measurements which are implemented in a feed forward loop in the control design. The main function of the MRU is to feed the control system with heave measurements for heave movement cancellation, isolating the drill string from the rig movements. This gives us the following controller.

$$u = v_{dr}(t) - v_{MRU} \quad (4.5)$$

where v_{MRU} follows the relationship expressed in Equation (4.1). The control design is displayed as a block diagram in Figure 4.2.

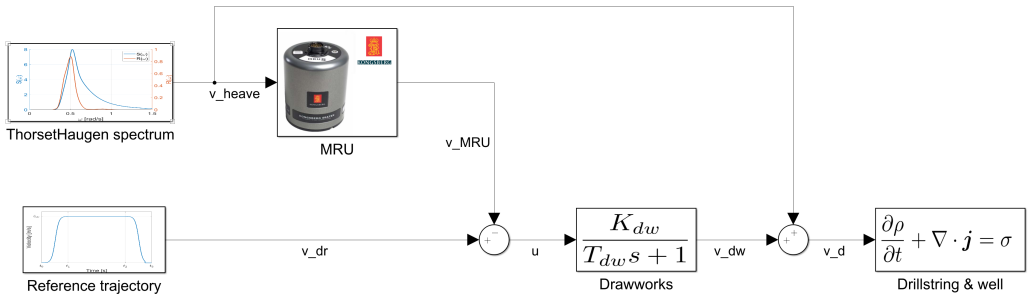


Figure 4.2: Control design Alpha block diagram.

Alpha simulation analysis

The first setting we want to simulate is the trivial case, where there are no waves present. In this case, as displayed in Figure 4.3, the drill string follows the reference trajectory with high accuracy. The pressure below the drilling bit is also displayed, and one may observe that the the delta pressure in this setting is $\Delta p_{bb} = 1.68$ Bar. In the forthcoming simulations, this value is interesting for comparison purposes to evaluate the performance of the different control designs. The next simulation included wave interaction to the rig, generated based on the Torsethaugen spectrum discussed in Chapter 3, and is displayed in Figure 4.4. The delta pressure was observed to be $\Delta p_{bb} = 3.24$ Bar and the tripping velocity error RMS $\bar{e}_d = 0.0293$ m/s.

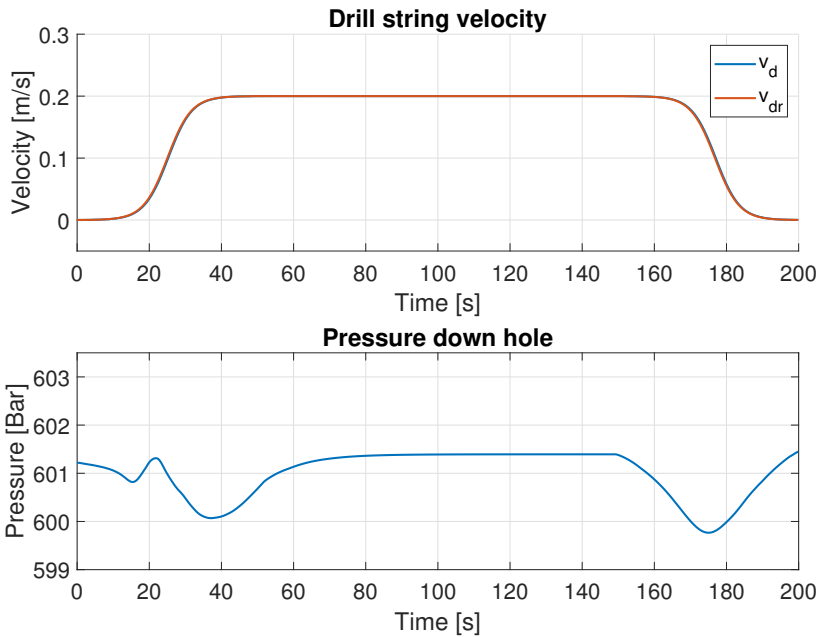


Figure 4.3: Alpha simulation without wave interaction measured $\bar{e}_d = 1.05 \cdot 10^{-3}$ m/s and $\Delta p_{bb} = 1.68$ Bar.

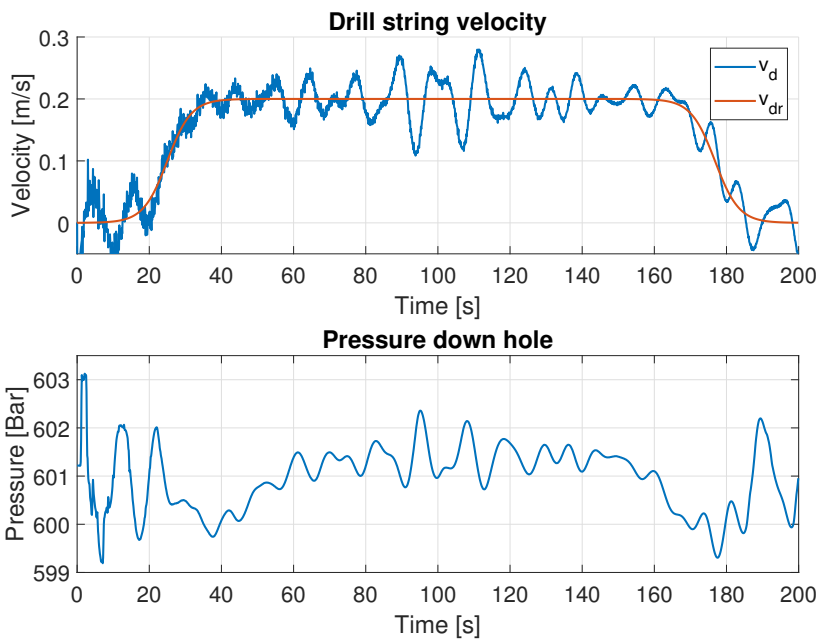


Figure 4.4: Alpha simulation with wave interaction measured $\bar{v}_d = 0.0293$ m/s and $\Delta p_{bb} = 3.93$ Bar.

4.3.2 Bravo design

The next control design is an augmentation of the Alpha control design. Since the Alpha control design is only based on encoder measurements, we propose a more robust control design where a drill string velocity feedback loop is introduced. The drill string velocity can be estimated based on the measured hook load, with the following linearized expression

$$v_d(F_{hl}) = C_1 F_{hl} + C_2 F_{hl,0} \quad (4.6)$$

where C_1 and C_2 are linearization coefficients, F_{hl} is the measured hook load, and $F_{hl,0}$ is the static hook load. For this control design, the tripping velocity error, \tilde{v}_d , will be considered. The tripping velocity error is expressed as

$$\tilde{v}_d = v_{dr} - v_d \quad (4.7)$$

which is used as an input to a proportional - integral (PI) controller. The proportional term will scale the output, u_c , based on the magnitude of the error, whereas the integral term will ensure no steady state errors in the system. Mathematically, we express this as

$$\lim_{t \rightarrow \infty} \tilde{v}_d(t) = 0 \quad (4.8)$$

The PI controller with the disturbance feed forward loop from the MRU takes the following form.

$$u = \underbrace{K_p \left(\tilde{v}_d + \frac{1}{T_i} \int_0^t \tilde{v}_d(\tau) d\tau \right)}_{\text{PI controller}} - \underbrace{v_{MRU}}_{\text{Disturbance feed forward}} \quad (4.9)$$

where K_p and T_i are tuning parameters. Applying the Laplace transform of the PI controller yields the transfer function from the tripping velocity error to the controller output.

$$H_u(s) = \frac{u_c}{\tilde{v}_d}(s) = K_p \frac{1 + T_i s}{T_i s} \quad (4.10)$$

The tuning parameter K_p was chosen as

$$K_p = \frac{u_c^{max}}{\tilde{v}_d^{max}} \quad (4.11)$$

where u_c^{max} and \tilde{v}_d^{max} are the expected maximum values for the control input and the tripping velocity error, respectively. The integral time, T_i , was chosen based on trail and error on the case without waves to eliminate steady state error. The Bravo control design is displayed in Figure 4.5.

When this control design was tested in simulation, the hook load measurements turned out to be contaminated with a high frequency noise. In fact, the amount of noise on the signal rendered the system unstable for a relatively low choice of tuning parameters. To work around this problem, a second order low pass filter was implemented in order to damp out the high frequencies in the measurements. The filter has the form

$$H_{lp}(s) = \frac{\hat{F}_{hl}}{F_{hl}}(s) = \frac{\omega_c^2}{s^2 + 2\zeta\omega_c s + \omega_c^2} \quad (4.12)$$

where the cutoff frequency ω_c and the relative damping factor ζ was chosen appropriately based on the frequencies in the noise.

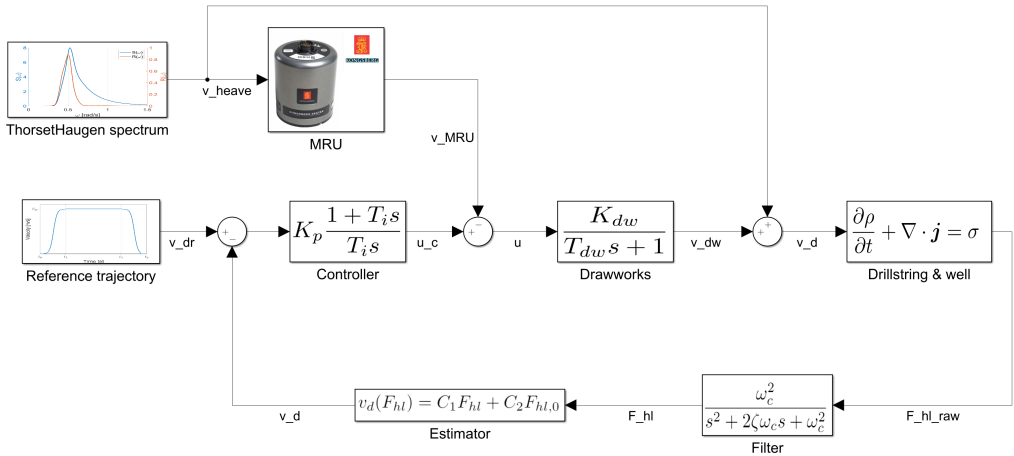


Figure 4.5: Control design Bravo block diagram.

Simulation analysis Bravo

As with the Alpha design, both the cases with and without wave interaction were simulated. The simulation results for the case without wave interaction can be viewed in Figure 4.6. One may observe that the tripping velocity does not follow the reference quite as accurately as the Alpha design. Too high proportional gain, K_p , rendered the system unstable for the case with wave interaction. The reason for the instability originates from the left over noise in the feedback signal getting amplified by the controller gain, introducing an even higher oscillation of the drill string. Therefore, the gain was turned down and the integral time, T_i , was adjusted so that there was no steady state error while tripping. Moving over to the pressure plot in Figure 4.6, the delta pressure was reduced by a factor of 3.5% compared to the Alpha design. Even though this is not a significant number, one may observe that the pressure does not fall as low during the acceleration phase as with the alpha design. This is due to the slower convergence of the Bravo controller, smoothing out the "corners" in the trajectory. This motivates the idea for an even smoother trajectory where the jerk of the tripping trajectory has a lower absolute value.¹ Further testing takes place later in this chapter with different tripping velocities.

Next, the case with waves was simulated with the Bravo control design. The tripping velocity error RMS value increased by a factor of 27 % and the delta pressure increased by a factor of about 2%. The increase of the error RMS value is possibly due to the slower control design, not keeping up with the waves. This can be seen around $t = 100$ s, there were multiple high waves hitting the rig, and one may observe that the Alpha design is better at damping the motion of these waves. The increase in delta pressure is too small to speculate in, but greater advantages or disadvantages might arise in later simulations with different wave heights and tripping velocities.

¹Yerk is the change in acceleration wrt. time.

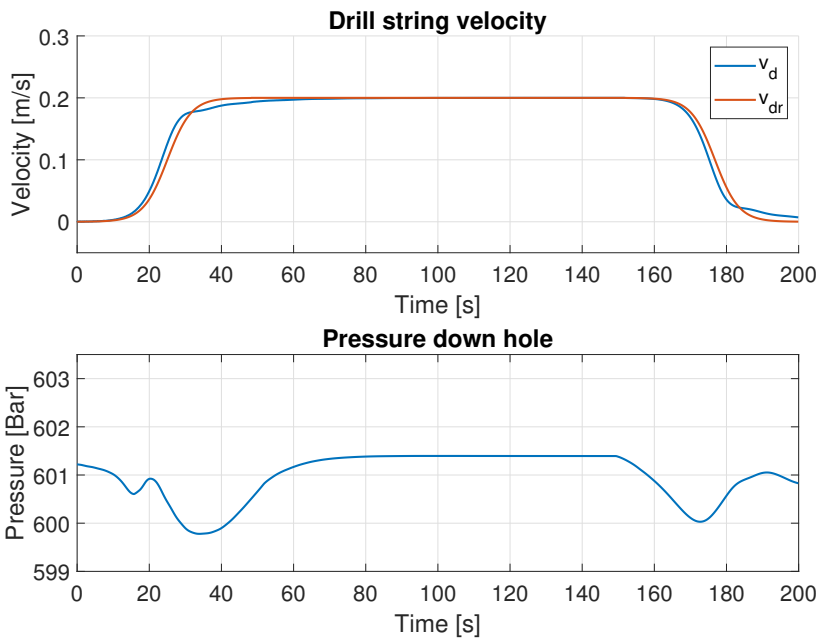


Figure 4.6: Bravo simulation without wave interaction measured $\bar{e}_d = 0.00798$ m/s and $\Delta p_{bb} = 1.62$ Bar.

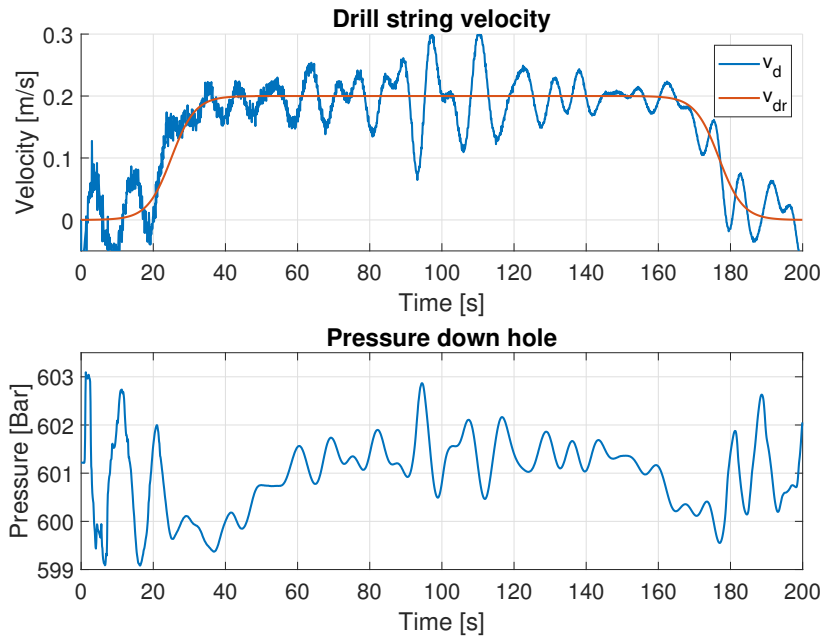


Figure 4.7: Bravo simulation with wave interaction measured $\bar{e}_d = 0.0375$ m/s and $\Delta p_{bb} = 4.01$ Bar.

4.3.3 Charlie design

The last control design to be discussed in this work is yet another augmentation, now based on the Bravo design. In the Bravo design, the hook load measurements were used to estimate the velocity of the drill string. As an added feature, we propose a damping term in our control design based on the time derivative of the hook load. Since our objective is to have a constant tripping velocity, the hook load should be constant when the reference trajectory is not commanding an acceleration. Thus, the time derivative of the hook load should be zero when the reference is not commanding an acceleration of the drill string. Mathematically, we write this as

$$\dot{F}_{hl}(t) = 0 \quad \forall t | (v_{dr}(t) = \hat{v}_{dr}) \quad (4.13)$$

The time derivative of the filtered hook load, denoted as $\dot{\hat{F}}_{hl}$, is acquired by convolving the filtered hook load with the following first order low pass filter with a bounded derivative. The transfer function is expressed as

$$H_{lp}(s) = \frac{\dot{\hat{F}}_{hl}(s)}{\hat{F}_{hl}(s)} = \frac{s}{T_{lp}s + 1} \quad (4.14)$$

where T_{lp} is the time constant of the filter. The PID controller with the disturbance feed forward from the MRU takes the following form.

$$u = \underbrace{K_p \left(\tilde{v}_d + \frac{1}{T_i} \int_0^t \tilde{v}_d(\tau) d\tau + T_d \frac{d}{dt} \hat{F}_{hl}(t) \right)}_{\text{PID controller}} - \underbrace{v_{MRU}}_{\text{Disturbance feed forward}} \quad (4.15)$$

The Charlie control design is displayed in Figure 4.8.

Simulation analysis Charlie

The overall performance of the Charlie control design is very similar to the Bravo design, and can be viewed in Figure 4.9 and Figure 4.10. As the largest pressure fluctuations down hole occurs during the high jerk phases, the delta pressure is pretty much unchanged as the damping only affects the constant velocity phase. Another reason for the performance similarities is the low derivative gain, T_d . This value had to be chosen quite low for the same reason as with the proportional gain. Even though the hook load signal is filtered, and the derivative is acquired with a low pass filter, the derivative of the hook load signal, $\dot{\hat{F}}_{hl}$, is too noisy to make any significant impact to the control design with the particular choice of filters discussed in this work.

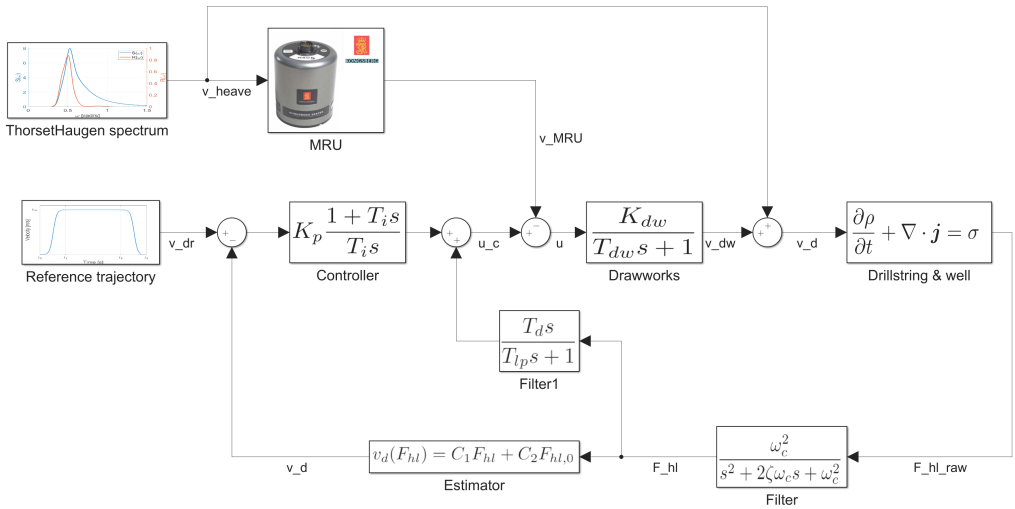


Figure 4.8: Control design Charlie block diagram.

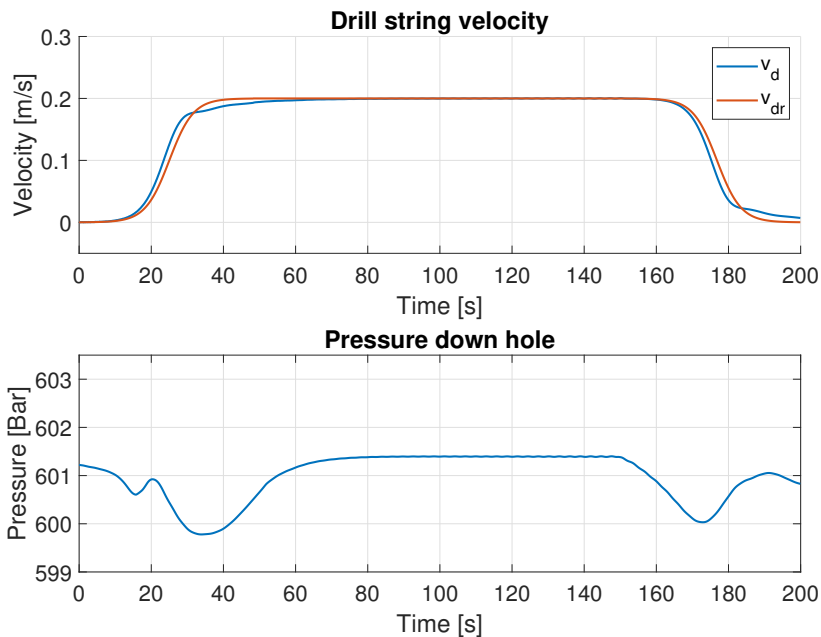


Figure 4.9: Charlie simulation without wave interaction measured $\bar{e}_d = 0.00797$ m/s and $\Delta p_{bb} = 1.62$ Bar.

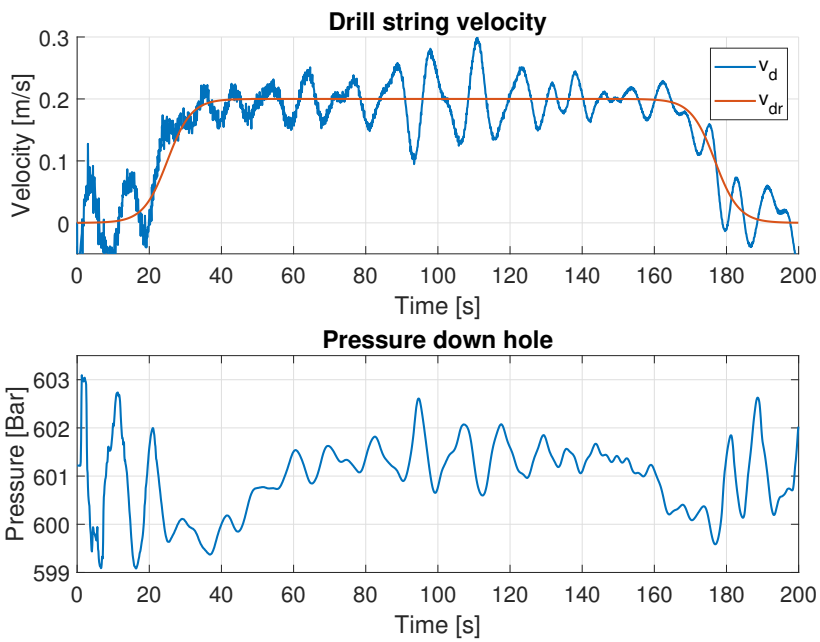


Figure 4.10: Alpha simulation with wave interaction measured $\bar{e}_d = 0.0351$ m/s and $\Delta p_{bb} = 4.01$ Bar.

4.3.4 Control design comparison

In order to compare the three control designs, a series of simulations were performed where the following variables were changed from the setup in the previous simulations. First, the tripping velocity \hat{v}_{dr} was set to vary from 0.1 m/s to 0.5 m/s. Then, the significant wave height H_s was set to go between 2 meters and 10 meters. Finally, the drawworks time constant T_{dw} varied from 0.1 seconds to 0.5 seconds. For all the simulations, the delta pressure Δp_{bb} and the tripping velocity error RMS \bar{e}_d were recorded, and are displayed in Figure 4.11. Observing the first row in the figure, one may notice that the delta pressure is

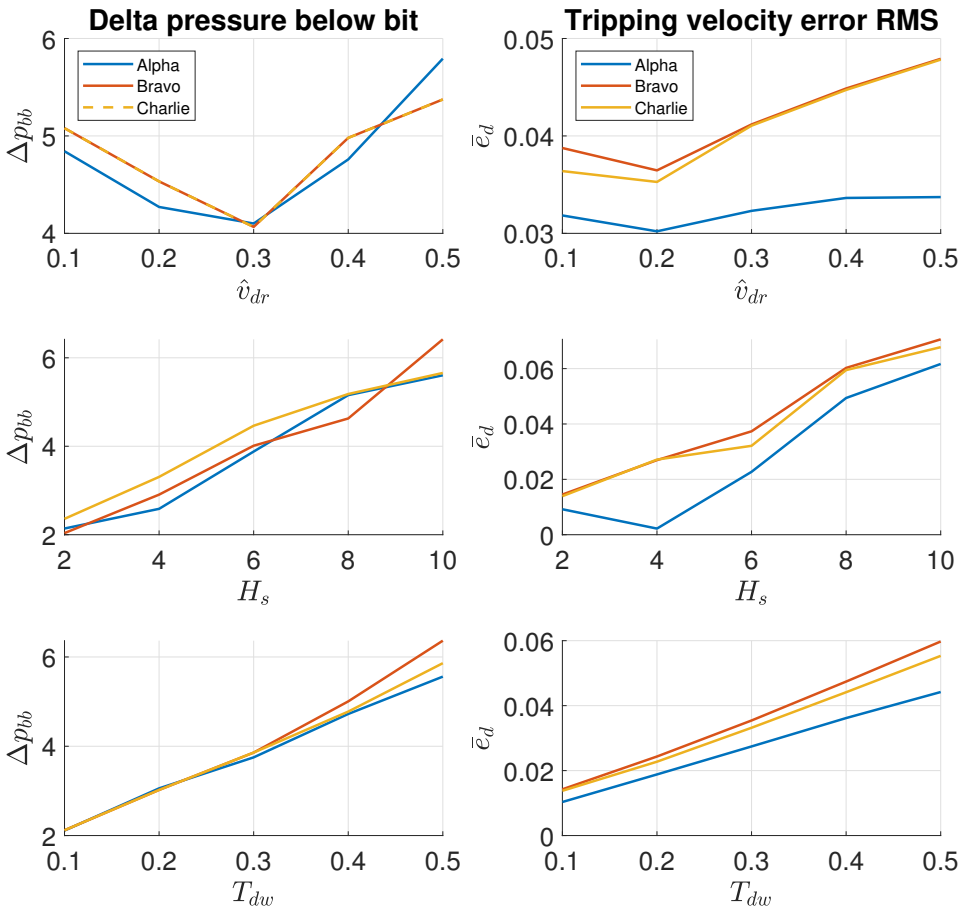


Figure 4.11: Control design comparison with multiple parameter variations.

at its lowest point for a tripping velocity of 0.3 m/s. Since the controllers were tuned for a tripping velocity of 0.2 m/s, the simulations with lower tripping velocity did not perform as well as one would expect. A controller with gain scheduling could have solved the problem if the system should operate on different tripping velocities. One could expect an increased delta pressure with higher tripping velocity. This observation, once again, motivates for

an even smoother trajectory with a lower acceleration if a delta pressure reduction should be achieved. Moving along to the error plot, it is clear that the Alpha design follows the reference trajectory with the highest accuracy. As discussed earlier, the slow converging controllers are leaving greater errors for an increase of tripping velocity. On the second row in the figure, the significant wave height simulations are displayed. It should be expected that the delta pressure would increase with higher waves, as this represents a more difficult drilling condition. Once again, the Alpha design leaves the lowest delta pressures and the smallest errors, arguing for an advantage of the Alpha design for the different wave heights. Lastly, in the third row, the simulations with different drawworks time constants are displayed. The great increase in delta pressure for a higher time constant motivates the fact that a slow hoisting system could lead to severe delta pressures down hole when used for heave compensation. That being said, it is worth noting that the Charlie design perform better than the Bravo design, both for delta pressure and tripping velocity error. This might be due to the damping term damping out the great oscillations which are generated when the hoisting system is not keeping up with the waves.

Conclusion

In this work, we have seen the simplest control design outperforming the more sophisticated ones. Even though the Alpha design performed better, the delta pressure that was observed during simulation was far greater than the bench mark of $\Delta p_{bb} < 2.5$ bar. It can be argued that a more advanced pressure control design that utilized the fluid control devices could have reduced the delta pressure. We have also seen that the maximum tripping velocity is not as an important parameter as the tripping acceleration, in order to get low pressure fluctuations down hole. In future work, different types of trajectories could be tried out to minimize the pressure fluctuation during tripping. Further, one could argue that the more sophisticated designs would have gained performance if the measurements were filtered in a better way. For example by using a Kalman filter, the high oscillations could have been filtered out more efficiently without introducing a significant phase shift in the system. In future work, one could also be interested in a more detailed model of the hoisting system such that the saturation limits would be withheld. If such a model was implemented, one could be interested in trying out a control design that used power consumption measurements of the motor to analyze the heave motion. This type of control design could have a faster convergence than those based on pure hook load measurements, and could yield better results for heave compensation.

Bibliography

- [1] Bakerhughes, 2018. Principles of directional and horizontal drilling.
URL <https://global.shopbakerhughes.com/>
- [2] Cayeux, E., Skadsem, H. J., 2015. Accuracy and correction of hook load measurements during drilling operations. Society of Petroleum Engineers. doi:10.2118/173035-MS.
- [3] Cayeux, E., Sælevik, G., 2014. Evaluation of hook-load measurements in drilling rig hoisting systems. SINTEF-7020384/04/14.
- [4] Egeland, O., Gravdahl, T., 2003. Modelling and simulation for automatic control. Marine Cybernetics AS.
- [5] Fossen, T. I., 2011. Handbook of Marine Craft Hydrodynamics and Motion Control. John Wiley Sons, Ltd.
- [6] Godhavn, J.-M., 2010. Control requirements for automatic managed pressure drilling system. Society of Petroleum Engineers. doi:10.2118/119442-PA.
- [7] Greenfield, W., Lubinski, A., 1967. Use of bumper subs when drilling from floating vessels. Society of Petroleum Engineers. doi:10.2118/1549-PA.
- [8] J.G. Balchen, T. Andresen, B. F., 2003. Reguleringssteknikk, 5. utgave. Institutt for teknisk kybernetikk, NTNU, Trondheim.
- [9] Kongsberg, S., 2018. The ideal marine motion sensor.
URL <https://www.km.kongsberg.com>
- [10] Mitchell, R., 1988. Dynamic surge/swab pressure predictions. Society of Petroleum Engineers. doi:10.2118/16156-PA.
- [11] Strecker, T., Aamo, O. M., 2016. Rejecting pressure fluctuations induced by string movement in drilling. IFAC-PapersOnLine 49-8 (2016) 124–129.
- [12] Strecker, T., Aamo, O. M., 2017. Attenuating heave-induced pressure oscillations in offshore drilling by downhole flow control.

-
- [13] Strecker, T., Aamo, O. M., 2017. Simulation of heave-induced pressure oscillations in herschel-bulkley muds. Society of Petroleum Engineers. doi:10.2118/185947-PA.
- [14] Thorsethaugen, K., 1996. Model for a doubly peaked wave spectrum. SINTEF report STF22 A, 96204.
- [15] Varco, N. O., 2018. Automated drawwoks system (ads).
URL https://www.nov.com/Segments/Rig_Systems/Land/Hoisting/Drawworks/Drilling_Drawworks.aspx
- [16] Øyvind Breyholtz, G. N., Nikolaou, M., 2010. Automatic control of managed pressure drilling. Published in: Proceedings of the 2010 American Control Conference. INSPEC: 11509043.